

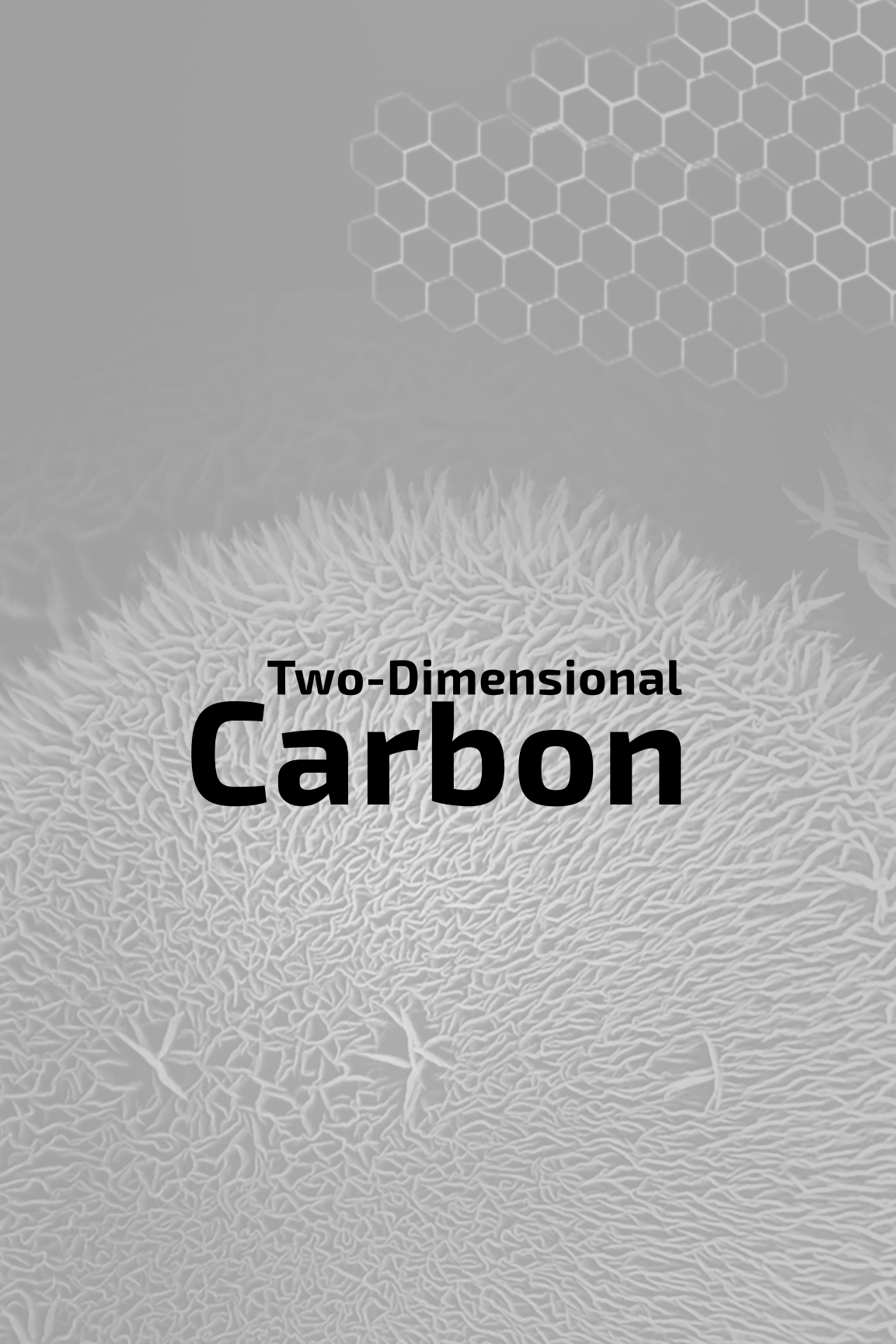
edited by
Yihong Wu
Zexiang Shen
Ting Yu



Two-Dimensional Carbon

Fundamental Properties, Synthesis,
Characterization, and Applications



The background features a light gray hexagonal lattice pattern in the upper right corner, transitioning into a dense, textured field of carbon nanotubes that fills the lower two-thirds of the image. The overall color palette is monochromatic, using shades of gray.

Two-Dimensional Carbon

This page intentionally left blank

edited by
Yihong Wu
Zexiang Shen
Ting Yu

Two-Dimensional Carbon

Fundamental Properties, Synthesis,
Characterization, and Applications

PAN STANFORD  PUBLISHING

CRC Press
Taylor & Francis Group
6000 Broken Sound Parkway NW, Suite 300
Boca Raton, FL 33487-2742

© 2014 by Taylor & Francis Group, LLC
CRC Press is an imprint of Taylor & Francis Group, an Informa business

No claim to original U.S. Government works
Version Date: 20140318

International Standard Book Number-13: 978-981-4411-95-0 (eBook - PDF)

This book contains information obtained from authentic and highly regarded sources. Reasonable efforts have been made to publish reliable data and information, but the author and publisher cannot assume responsibility for the validity of all materials or the consequences of their use. The authors and publishers have attempted to trace the copyright holders of all material reproduced in this publication and apologize to copyright holders if permission to publish in this form has not been obtained. If any copyright material has not been acknowledged please write and let us know so we may rectify in any future reprint.

Except as permitted under U.S. Copyright Law, no part of this book may be reprinted, reproduced, transmitted, or utilized in any form by any electronic, mechanical, or other means, now known or hereafter invented, including photocopying, microfilming, and recording, or in any information storage or retrieval system, without written permission from the publishers.

For permission to photocopy or use material electronically from this work, please access www.copyright.com (<http://www.copyright.com/>) or contact the Copyright Clearance Center, Inc. (CCC), 222 Rosewood Drive, Danvers, MA 01923, 978-750-8400. CCC is a not-for-profit organization that provides licenses and registration for a variety of users. For organizations that have been granted a photocopy license by the CCC, a separate system of payment has been arranged.

Trademark Notice: Product or corporate names may be trademarks or registered trademarks, and are used only for identification and explanation without intent to infringe.

Visit the Taylor & Francis Web site at
<http://www.taylorandfrancis.com>

and the CRC Press Web site at
<http://www.crcpress.com>

Contents

<i>Preface</i>	xi
1. Introduction	1
<i>Yihong Wu</i>	
1.1 Carbon Allotropes	1
1.2 Two-Dimensional Carbon	3
1.3 Scope of This Book	4
2. Electronic Band Structure and Properties of Graphene	11
<i>Yihong Wu</i>	
2.1 Lattice structure	11
2.2 Electronic Band Structure	12
2.2.1 Tight-Binding Model	12
2.2.2 Low-Energy Electronic Spectrum	15
2.2.3 Effect of Magnetic Field	19
2.2.4 Quantum Confinement and Tunneling	20
2.3 Electrical Transport Properties	23
2.3.1 Weak (Weak Anti-) Localization	24
2.3.2 Electrical Conductivity and Mobility	26
2.4 Summary	29
3. Growth of Epitaxial Graphene on SiC	35
<i>Xiaosong Wu</i>	
3.1 Introduction	36
3.1.1 Graphene	36
3.1.2 Epitaxial Graphene on SiC	37
3.2 Growth on Si-Face	39
3.2.1 Growth Mechanism	39
3.2.2 Control the Growth	42
3.2.3 Beyond One Layer	46
3.2.4 More Than Just Si Desorption	47
3.3 Growth on C-Face	49
3.4 Conclusion	56

4. Chemical Vapor Deposition of Large-Area Graphene on Metallic Substrates	67
<i>Wei Wu and Qingkai Yu</i>	
4.1 Introduction	67
4.2 Graphene Synthesis Methods	68
4.2.1 Mechanical Exfoliation	68
4.2.2 Graphite Oxide Reduction	69
4.2.3 Thermal Decomposition of SiC	69
4.2.4 CVD of Hydrocarbons on Metals	70
4.3 CVD Graphene on Nickel	70
4.4 CVD Graphene on Copper	78
4.5 Single-Crystal Graphene	84
4.6 Summary	88
5. Growth and Electrical Characterization of Carbon Nanowalls	95
<i>Yihong Wu</i>	
5.1 Introduction	95
5.2 Synthesis of Carbon Nanowalls by MPECVD	96
5.2.1 Growth Apparatus and Surface Morphology	96
5.2.2 Growth Mechanism	99
5.3 Electrical Transport Properties	100
5.3.1 Electrical Transport Across the CNW Junctions	102
5.3.2 Electrical Transport in Carbon–Metal Point-Contact	106
5.4 Magnetic Properties	114
5.5 Summary	116
6. Structural Characterization of Carbon Nanowalls and Their Potential Applications in Energy Devices	121
<i>Masaru Tachibana</i>	
6.1 Introduction	122
6.2 Synthesis of CNWs	123
6.3 Structural Characterization of CNWS	124
6.3.1 Raman Spectroscopy	125
6.3.2 Transmission Electron Microscopy	129
6.4 Potential Applications of CNWs to Energy Devices	134

6.4.1	CNWs as Negative Electrode in Lithium Ion Battery	134
6.4.1.1	Preparation of electrode	135
6.4.1.2	Cyclic voltammogram	135
6.4.1.3	Charge/discharge curve	137
6.4.1.4	High rate property	138
6.4.1.5	CNWs as catalyst support in fuel cell	140
6.4.1.6	Preparation of Pt/CNW	140
6.4.1.7	Physical characterization of Pt/CNW	141
6.4.1.8	Electrochemical characterization of Pt/CNW	144
6.5	Summary	146
7.	Raman and Infrared Spectroscopic Characterization of Graphene	153
	<i>Da Zhan and Zexiang Shen</i>	
7.1	Introduction	153
7.2	Raman Spectroscopic Features of Graphene	154
7.2.1	Identify the Thickness and Stacking Geometry of Graphene	155
7.2.2	Probing Doped Charges in Graphene	159
7.2.3	Defects in Graphene Probed by Raman Spectroscopy	164
7.2.4	Graphene Edge Chirality Identified by Raman Spectroscopy	169
7.2.5	Raman Spectroscopy Probes Strain in Graphene	173
7.3	Chemical Functional Groups and Energy Gaps of Graphene Probed by Infrared Spectroscopy	174
7.4	Summary	176
8.	Graphene-Based Materials for Electrochemical Energy Storage	183
	<i>Jintao Zhang and Xiu Song Zhao</i>	
8.1	Introduction	183
8.1.1	A Family of Graphene-Based Materials	184
8.1.2	Electrochemical Energy Storage Systems	187

8.2	Synthesis of Graphene-Based Materials	190
8.2.1	Synthesis of Graphene	190
8.2.2	Synthesis of Chemically Modified Graphene	195
8.2.3	Synthesis of Graphene-Based Composite Materials	202
8.3	Graphene-Based Materials as Supercapacitor Electrodes	207
8.3.1	Energy Storage in Supercapacitor	207
8.3.2	Basic Principles and Techniques for Evaluation of Supercapacitor	210
8.3.3	Graphene and Reduced Graphene Oxide as Supercapacitor Electrodes	216
8.3.4	Graphene Based Composite Materials as Supercapacitor Electrodes	223
8.4	Summary and Perspectives	232
8.5	Acknowledgements	233
9.	Chemical Synthesis of Graphene and Its Applications in Batteries	247
	<i>Xufeng Zhou and Zhaoping Liu</i>	
9.1	Introduction	247
9.2	Chemical Synthesis of Graphene	248
9.2.1	Direct Exfoliation of Graphite	248
9.2.2	Graphene from Graphite Oxide	249
9.2.3	Graphene from Graphite Intercalated Compounds	254
9.3	Applications of Graphene in Batteries	256
9.3.1	Li ion Batteries	256
9.3.2	Supercapacitors	264
9.3.3	Other types of Batteries	269
9.4	Summary	271
10.	Photonic Properties of Graphene Device	279
	<i>Hua-Min Li and Won Jong Yoo</i>	
10.1	Introduction	280
10.2	Energy Band Structure of Graphene	283
10.3	Photonic Absorption of Graphene	284
10.4	Photocurrent Generation in Graphene	286
10.5	Technology for Performance Improvement	289

10.5.1	Asymmetric Metallization	290
10.5.2	Graphene Stack Channel	290
10.5.3	Graphene Plasmonics	291
10.6	Summary	292
11.	Graphene Oxides and Reduced Graphene Oxide Sheets: Synthesis, Characterization, Fundamental Properties, and Applications	297
	<i>Shixin Wu and Hua Zhang</i>	
11.1	Introduction	297
11.2	Methods of Production of Graphene	298
11.3	Introduction to Graphene Oxide	299
11.4	Methods to Produce Stable Dispersion of Reduced Graphene Oxide	300
11.5	Characterizations and Fundamental Properties of Reduced Graphene Oxide	302
11.5.1	Characterization with Atomic Force Microscopy	302
11.5.2	Characterization with X-Ray Diffraction	303
11.5.3	Characterization with X-Ray Photoelectron Spectroscopy (XPS)	304
11.5.4	Characterization with Raman Spectroscopy	305
11.5.5	Conductivity	305
11.6	Sensing Applications of Reduced Graphene Oxide	306
11.6.1	Field-Effect Transistor Sensors	306
11.6.2	Electrochemical Sensors	308
11.6.3	Matrices for Mass Spectrometry	309
11.7	Device Applications of Reduced Graphene Oxide	310
11.7.1	Memory Devices	310
11.7.2	Solar Cells	310
11.8	Applications of Graphene Oxide	313
11.8.1	Fluorescence Sensors	313
11.8.2	Solar Cells	315
11.9	Conclusion	316
	<i>Index</i>	329

This page intentionally left blank

Preface

Graphene in the ideal form is a single layer of carbon atoms arranged in a honeycomb lattice, consisting of two interpenetrating Bravais sublattices. It is this unique lattice structure that gives graphene a range of peculiar properties that most metals and semiconductors lack. As far as electronic applications are concerned, its gapless and linear energy spectrum, high carrier mobility, frequency-independent absorption, and long spin diffusion length make it a material of choice for a variety of electronic, photonic, and spintronic devices. Apart from these applications, owing to its unique electronic properties, graphene has also attracted tremendous attention for applications that are due to primarily its unique shape and surface morphology, and low-cost production of related materials such as few-layer graphene sheets and graphene oxides. These graphene derivatives are more attractive and viable than single-layer graphene for applications that require a large quantity of materials with low cost and that rely less on graphene's electronic properties. These different types of graphene-based carbon nanostructures are referred to as two-dimensional (2D) carbon in this book, which include but are not limited to single layer graphene, few-layer graphene, vertically aligned few-layer graphene sheets (or carbon nanowalls), reduced graphene oxide and graphene oxide, etc. As far as large-scale applications are concerned, we feel that these graphene-related materials may be a step closer to reality than their pure graphene counterpart, in particular, in energy storage-related applications. This has motivated us to pull together a team of researchers who are doing frontier research in the respective fields to discuss fundamental properties of graphene, synthesis and characterization of graphene and related 2D carbon structures, and associated applications in an edited book.

The book is organized into 11 chapters. Following the introduction in Chapter 1, Yihong Wu gives a brief overview of electronic band structure and properties of graphene in Chapter 2. In addition to the description of band structure based on the tight-binding model, several unique electron transport properties of graphene are discussed. Chapters 3 and 4 cover the growth of graphene on

SiC substrates by Xiaosong Wu and on metallic substrates by Wei Wu and Qingkai Yu, respectively. The former discusses the growth mechanism of graphene on both Si-face and C-face of SiC, while the latter deals with the growth of graphene on nickel and copper substrates using chemical vapor deposition. Chapter 5 discusses the growth and electrical transport properties of carbon nanowalls on different types of substrates. Emphases are placed on how to design and form different types of electrical contacts that allow for the study of electrical transport properties of material structures with an unusual surface morphology. This is then followed by Chapter 6, in which Masaru Tachibana writes about the structural characterization of carbon nanowalls using Raman spectroscopy and transmission electron microscopy, and their potential applications in energy storage such as lithium ion batteries and fuel cells. In Chapter 7, Zexiang Shen and Da Zhan discuss the structural properties of 2D carbon based on Raman spectroscopy studies. Chapters 8 and 9 are devoted to the energy storage applications of graphene obtained by the chemical reduction route, which is more cost effective compared with other vapor deposition-based techniques. Xiu Song Zhao and Jintao Zhang focus on the applications of 2D carbon in supercapacitor in Chapter 8, followed by Zhaoping Liu and Xufeng Zhou dealing with battery applications in Chapter 9. The photonic properties of graphene are discussed by Won Jong Yoo and Hua-Min Li in Chapter 10. In Chapter 11, Hua Zhang and Shixin Wu discuss another important material derived from graphene, graphene oxide, and its potential applications in sensor and memory devices.

Owing to the very competitive environment of graphene research, many researchers would put their priority in doing research and writing papers rather than contributing to book chapters. In this context, we would like to thank all the contributing authors for their excellent chapters; without their extra efforts, we would not have the book in the present form. We would like to thank Prof. Andrew Thye Shen Wee of National University of Singapore for giving the opportunity to edit this book. Finally, we would like to thank Mr. Stanford Chong and his team at Pan Stanford Publishing for their help on this project.

Yihong Wu
Zexiang Shen
Ting Yu

Chapter 1

Introduction

Yihong Wu

*Department of Electrical and Computer Engineering,
National University of Singapore, 4 Engineering Drive 3,
Singapore 117576
elewuyh@nus.edu.sg*

1.1 Carbon Allotropes

The properties of a material at the mesoscopic scale are determined not only by the nature of its chemical bonds but also by its dimensionality and shape. This is particularly true for carbon-based materials. In the ground state, the carbon atom has four valence electrons, two in the 2s sub-shell and two in the 2p sub-shell. When a large number of carbon atoms come together to form materials under appropriate conditions, an individual carbon atom will promote one of its 2s electrons into its empty 2p orbital and then form bonds with other carbon atoms via sp hybrid orbitals. Depending on the number of p orbitals (1 to 3) mixing with the s orbital, it will lead to the formation of three kinds of sp hybrid orbitals called sp, sp², and sp³. Carbon atoms with sp² and sp³ hybrid orbitals are able to form

Two-Dimensional Carbon: Fundamental Properties, Synthesis, Characterization, and Applications

Edited by Yihong Wu, Zexiang Shen, and Ting Yu

Copyright © 2014 Pan Stanford Publishing Pte. Ltd.

ISBN 978-981-4411-94-3 (Hardcover), 978-981-4411-95-0 (eBook)

www.panstanford.com

three and four bonds with neighboring carbon atoms, respectively, which form the bases of graphene and diamond.

An ideal graphene is a monatomic layer of carbon atoms arranged in a honeycomb lattice; therefore, graphene is a perfect two-dimensional (2D) material in the ideal case. As ideal 2D crystals in free state are unstable at finite temperature [1], graphene tends to evolve into other types of structures with enhanced structural stability, such as graphite, fullerene, nanotubes, and their derivatives [2]. Graphite is formed by the layering of a large number of graphene layers mediated by the van der Waals force; therefore, from the point of view of physics, it falls into the category of three-dimensional (3D) systems. Under appropriate conditions, a single- or multiple-layer graphene can also roll up along certain directions to form a tubular structure called carbon nanotubes (CNTs) [3]. The CNTs, which can be in the form of single-walled, double-walled, and multiple-walled structures, are considered one-dimensional (1D) objects as far as their physical properties are concerned [4]. With the introduction of pentagons, graphene can also be wrapped up to form zero-dimensional (0D) fullerenes [5]. In addition to cylindrical CNTs and spherical fullerenes, there also exist intermediate carbon nanoforms, such as nanocones with different stacking structures [6]. Although ideal graphene is unstable, it may become stable through the introduction of local curvatures, as discussed in [7], or through the support of foreign materials. Macroscopic single-layer graphene was successfully isolated from graphite through mechanical exfoliation in 2004 and was found to be stable on a foreign substrate, highly crystalline, and chemically inert under ambient conditions [8–10], albeit with local roughness and ripples [11]. This discovery has led to an explosive interest in 2D carbon nanostructures, which also earned K. S. Novoselov and A. K. Geim the 2010 Nobel Prize in Physics. In addition to crystalline carbon allotropes, there are also amorphous carbons and carbons with mixed phases, such as activated carbon and diamond-like carbon (DLC). As far as large-scale industrial applications are concerned, bulk carbons are still dominant, although nanocarbons are expected to play an increasingly important role in future. A pictorial summary of different forms of single-phase carbon, or allotropes of carbon, is presented in Fig. 1.1. For a detailed discussion on nomenclature of sp^2 carbon nanoforms, the reader may refer to [6].

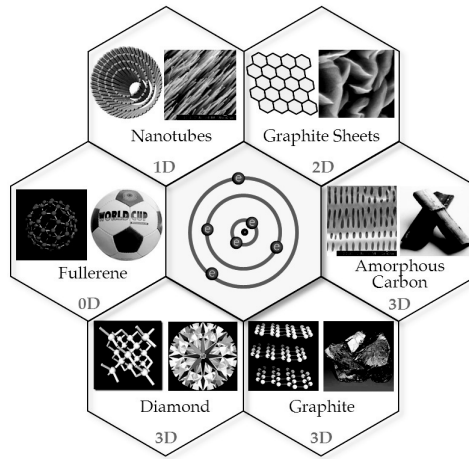


Figure 1.1 Major allotropes of carbon.

1.2 Two-Dimensional Carbon

Among all carbon allotropes, graphene stands out because of its unique lattice structure: a monatomic honeycomb lattice with a perfect 2D dimensionality. The specific lattice structure in combination with the valence electron configuration of carbon atoms gives rise to peculiar electronic band structures, which distinguish graphene from other allotropes. The quasi-particles (or electrons and holes) in graphene behave like massless relativistic particles, or Dirac fermions, with the electrons and holes degenerated at the Dirac points [12–16]. This gives rise to a number of peculiar physical properties that are either not found or superior to those found in other carbon allotropes [17]. Some of the unique physical phenomena that have been observed or explored so far include unconventional integer quantum Hall effect (IQHE) [9, 10], Klein tunneling [18–20], valley polarization [21, 22], universal (non-universal) minimum conductivity [23–26], weak (weak anti-) localization [23, 27–31], ultrahigh mobility [23, 32–34], specular Andreev reflection at the graphene–superconductor interface [35, 36], exceptional thermal conductivity [37, 38], and superior mechanical properties [39].

Since the discovery of single-layer graphene, tremendous progress has been made in the development/redevelopment of various types of techniques for synthesizing both single-layer graphene

(SLG) and few-layer graphene (FLG) sheets, such as epitaxial growth on both SiC and metallic substrates [40–44], reduction from graphite oxide [45], chemical vapor deposition (CVD) [7, 46–48], and electrical discharge [49]. It is worth noting that most of these techniques are not new and they have been used to grow various types of 2D graphitic materials before the discovery of graphene. Depending on the synthesis techniques and conditions, in addition to pure graphene, various secondary forms of graphene can also be formed. These carbon nanostructures are typically multilayer graphene with a varying degree of curvature, defects, and morphology. Although different terminologies have been introduced to describe these nano-carbon forms [6], in general, they can all be referred to as two-dimensional carbon, which is the focus of this book. Just like diamond and graphite, perfect crystalline materials are always desirable, but they are more difficult to produce and thus often too expensive for large-scale applications; on the contrary, partially perfect carbons such as synthetic graphite/diamond, activated carbon, and DLC are more widely used in industry. The same scenario may also happen to graphene, which warrants a book to discuss 2D carbon in a more inclusive manner instead of purely on graphene.

1.3 Scope of This Book

This book is not intended to focus on the fascinating properties of graphene that have already been covered by other books. Instead, after a brief introduction of the band structure and electronic properties of graphene, we focus more on the synthesis and characterization of 2D carbons in general and the associated applications, in particular, in the area of energy storage. Based on this spirit, this book is organized into 11 chapters. Following the introduction, Yihong Wu gives a brief overview of electronic band structure and properties of graphene in Chapter 2. In addition to the description of band structure based on the tight-binding model, several unique electron transport properties of graphene are discussed, including quantum Hall effect, weak (weak anti-) localization, and electrical conductivity and mobility. Chapters 3 and 4 cover the growth of graphene on SiC substrates by Xiaosong Wu and on metallic substrates by Qingkai Yu, respectively. The former discusses the growth mechanism of graphene on both Si-face and C-face of SiC, while the latter deals with the growth of graphene on nickel and copper substrates using CVD. Chapter 5

discusses the growth and electrical transport properties of carbon nanowalls on different types of substrates. Emphasis is placed on how to design and form different types of electrical contacts that allow for the study of electrical transport properties of material structures with an unusual surface morphology. This is then followed by Chapter 6, in which Masaru Tachibana writes about the structural characterization of carbon nanowalls using Raman spectroscopy and transmission electron microscopy, and their potential applications in energy storage such as lithium ion batteries and fuel cells. In Chapter 7, Zexiang Shen discusses the structural properties of 2D carbon based on Raman spectroscopy studies. Chapters 8 and 9 are devoted to the energy storage applications of graphene obtained by the chemical reduction route, which is more cost effective compared with other vapor deposition-based techniques. X. S. Zhao focuses on the applications of 2D carbon in supercapacitor in Chapter 8, followed by Zhaoping Liu dealing with battery applications in Chapter 9. The photonic properties of graphene are discussed by Yoo Won Jong in Chapter 10. In Chapter 11, Hua Zhang discusses another important material derived from graphene—graphene oxide—and its potential applications in sensor and memory devices.

The current interest in graphene is phenomenal, as evidenced by the large number of publications published in the last few years. Many reviews have been written on graphene, covering various aspects from fundamental physics and electronic properties [16, 23, 50–55] to material synthesis [40–45, 56, 57] and applications [58–62]. Several books with different emphases are already available. It is not possible for any book to cover all the relevant topics on graphene and related nanostructures. By extending the coverage to both flat and vertically aligned graphene sheets, it is hoped that this book can serve as a good reference for research on 2D carbon in general rather than graphene only.

References

1. Marder M.P. (2010) *Condensed Matter Physics*, 2nd ed, JohnWiley, Hoboken, New Jersey.
2. Dresselhaus M.S., Dresselhaus G., Eklund P.C. (1996) *Science of Fullerenes and Carbon Nanotubes*, Academic Press, San Diego.
3. Iijima S. (1991) Helical microtubules of graphitic carbon, *Nature*, **354**, 56–58.

4. Saito R., Dresselhaus G., Dresselhaus M.S. (1998) *Physical Properties of Carbon Nanotubes*, Imperial College Press, London.
5. Kroto H.W., Heath J.R., O'Brien S.C., Curl R.F., Smalley R.E. (1985) C-60: Buckminsterfullerene, *Nature*, **318**, 162–163.
6. Suarez-Martinez I., Grobert N., Ewels C.P. (2012) Nomenclature of sp² carbon nanoforms, *Carbon*, **50**, 741–747.
7. Wu Y.H., Yang B.J., Zong B.Y., et al. (2004) Carbon nanowalls and related materials, *J Mater Chem*, **14**, 469–477.
8. Novoselov K.S., Geim A.K., Morozov S.V., et al. (2004) Electric field effect in atomically thin carbon films, *Science*, **306**, 666–669.
9. Novoselov K.S., Geim A.K., Morozov S.V., et al. (2005) Two-dimensional gas of massless Dirac fermions in graphene, *Nature*, **438**, 197–200.
10. Zhang Y.B., Tan Y.W., Stormer H.L., Kim P. (2005) Experimental observation of the quantum Hall effect and Berry's phase in graphene, *Nature*, **438**, 201–204.
11. Fasolino A., Los J.H., Katsnelson M.I. (2007) Intrinsic ripples in graphene, *Nat Mater*, **6**, 858–861.
12. Wallace P.R. (1947) The band theory of graphite, *Phys Rev*, **71**, 622.
13. McClure J.W. (1957) Band structure of graphite and de Haas-van Alphen effect, *Phys Rev*, **108**, 612.
14. Slonczewski J.C. and Weiss P.R. (1958) Band structure of graphite, *Phys Rev*, **109**, 272.
15. Semenoff G.W. (1984) Condensed-matter simulation of a three-dimensional anomaly, *Phys Rev Lett*, **53**, 2449.
16. Neto A.H.C., Guinea F., Peres N.M.R., Novoselov K.S., Geim A.K. (2009) The electronic properties of graphene, *Rev Mod Phys*, **81**, 109–162.
17. Ando T., Fowler A.B., Stern F. (1982) Electronic properties of two-dimensional systems, *Rev Mod Phys*, **54**, 437–672.
18. Katsnelson M.I., Novoselov K.S., Geim A.K. (2006) Chiral tunnelling and the Klein paradox in graphene, *Nat Phys*, **2**, 620–625.
19. Beenakker C.W.J. (2008) Colloquium: Andreev reflection and Klein tunneling in graphene, *Rev Mod Phys*, **80**, 1337–1354.
20. Stander N., Huard B., Goldhaber-Gordon D. (2009) Evidence for Klein tunneling in graphene p-n junctions, *Phys Rev Lett*, **102**, 026807.
21. Rycerz A., Tworzydło J., Beenakker C.W.J. (2007) Valley filter and valley valve in graphene, *Nat Phys*, **3**, 172–175.
22. Cresti A., Grosso G., Parravicini G.P. (2008) Valley-valve effect and even-odd chain parity in p-n graphene junctions, *Phys Rev B*, **77**, 233402.

23. Geim A.K., Novoselov K.S. (2007) The rise of graphene, *Nat Mater*, **6**, 183–191.
24. Ando T., Zheng Y.S., Suzuura H. (2002) Dynamical conductivity and zero-mode anomaly in honeycomb lattices, *J Phys Soc Jpn*, **71**, 1318–1324.
25. Ziegler K. (2007) Minimal conductivity of graphene: Nonuniversal values from the Kubo formula, *Phys Rev B*, **75**, 233407.
26. Adam S., Hwang E.H., Galitski V.M., Das Sarma S. (2007) A self-consistent theory for graphene transport, *Proc Natl Acad Sci USA*, **104**, 18392–18397.
27. Suzuura H., Ando T. (2002) Crossover from symplectic to orthogonal class in a two-dimensional honeycomb lattice, *Phys Rev Lett*, **89**, 266603.
28. McCann E., Kechedzhi K., Fal'ko V.I., Suzuura H., Ando T., Altshuler B.L. (2006) Weak-localization magnetoresistance and valley symmetry in graphene, *Phys Rev Lett*, **97**, 146805.
29. Morozov S.V., Novoselov K.S., Katsnelson M.I., et al. (2006) Strong suppression of weak localization in graphene, *Phys Rev Lett*, **97**, 016801.
30. Tikhonenko F.V., Horsell D.W., Gorbachev R.V., Savchenko A.K. (2008) Weak localization in graphene flakes, *Phys Rev Lett*, **100**, 056802.
31. Wu X.S., Li X.B., Song Z.M., Berger C., de Heer W.A. (2007) Weak antilocalization in epitaxial graphene: Evidence for chiral electrons, *Phys Rev Lett*, **98**, 136801.
32. Bolotin K.I., Sikes K.J., Jiang Z., et al. (2008) Ultrahigh electron mobility in suspended graphene, *Solid State Commun*, **146**, 351–355.
33. Orlita M., Faugeras C., Plochocka P., et al. (2008) Approaching the Dirac point in high-mobility multilayer epitaxial graphene, *Phys Rev Lett*, **101**, 267601.
34. Du X., Skachko I., Barker A., Andrei E.Y. (2008) Approaching ballistic transport in suspended graphene, *Nat Nanotechnol*, **3**, 491–495.
35. Beenakker C.W.J. (2006) Specular Andreev reflection in graphene, *Phys Rev Lett*, **97**, 067007.
36. Zhang Q.Y., Fu D.Y., Wang B.G., Zhang R., Xing D.Y. (2008) Signals for specular Andreev reflection, *Phys Rev Lett*, **101**, 047005.
37. Balandin A.A., Ghosh S., Bao W., et al. (2008) Superior thermal conductivity of single-layer graphene, *Nano Lett*, **8**, 902–907.
38. Balandin A.A. (2011) Thermal properties of graphene and nanostructured carbon materials, *Nat Mater*, **10**, 569–581.

39. Lee C., Wei X., Kysar J.W., Hone J. (2008) Measurement of the elastic properties and intrinsic strength of monolayer graphene, *Science*, **321**, 385–388.
40. de Heer W.A., Berger C., Wu X.S., et al. (2007) Epitaxial graphene, *Solid State Commun*, **143**, 92–100.
41. Hass J., de Heer W.A., Conrad E.H. (2008) The growth and morphology of epitaxial multilayer graphene, *J Phys: Condens Matter*, **20**, 323202.
42. Gall N.R., Rut'kov E.V., Tontegode A.Y. (1997) Two dimensional graphite films on metals and their intercalation, *Int J Mod Phys B*, **11**, 1865–1911.
43. Oshima C., Nagashima A. (1997) Ultra-thin epitaxial films of graphite and hexagonal boron nitride on solid surfaces, *J Phys: Condens Matter*, **9**, 1–20.
44. Wintterlin J., Bocquet M.L. (2009) Graphene on metal surfaces, *Surf Sci*, **603**, 1841–1852.
45. Park S.J., Ruoff R.S. (2009) Chemical methods for the production of graphenes, *Nat Nanotechnol*, **4**, 217.
46. Wu Y.H., Qiao P.W., Chong T.C., Shen Z.X. (2002) Carbon nanowalls grown by microwave plasma enhanced chemical vapor deposition, *Adv Mater*, **14**, 64–67.
47. Wang J.J., Zhu M.Y., Outlaw R.A., et al. (2004) Free-standing subnanometer graphite sheets, *Appl Phys Lett*, **85**, 1265–1267.
48. Hiramatsu M., Shiji K., Amano H., Hori M. (2004) Fabrication of vertically aligned carbon nanowalls using capacitively coupled plasma-enhanced chemical vapor deposition assisted by hydrogen radical injection, *Appl Phys Lett*, **84**, 4708–4710.
49. Ebbesen T.W., Ajayan P.M. (1992) Large-scale synthesis of carbon nanotubes, *Nature*, **358**, 220–222.
50. Geim A.K., MacDonald A.H. (2007) Graphene: Exploring carbon flatland, *Phys Today*, **60**, 35–41.
51. Katsnelson M.I. (2007) Graphene: Carbon in two dimensions, *Materials Today*, **10**, 20–27.
52. Ando T. (2007) Exotic electronic and transport properties of graphene, *Physica E: Low-Dimensional Syst Nanostruct*, **40**, 213–227.
53. Ferrari A.C. (2007) Raman spectroscopy of graphene and graphite: Disorder, electron–phonon coupling, doping and nonadiabatic effects, *Solid State Commun*, **143**, 47–57.

54. Malard L.M., Pimenta M.A., Dresselhaus G., Dresselhaus M.S. (2009) Raman spectroscopy in graphene, *Phys Rep*, **473**, 51–87.
55. Molitor F., Guttinger J., Stampfer C., et al. (2011) Electronic properties of graphene nanostructures, *J Phys Condens Matter*, **23**, 243201.
56. Singh V., Joung D., Zhai L., Das S., Khondaker S.I., Seal S. (2011) Graphene based materials: Past, present and future, *Prog Mater Sci*, **56**, 1178–1271.
57. Wu Y.H., Yu T., Shen Z.X. (2010) Two-dimensional carbon nanostructures: Fundamental properties, synthesis, characterization, and potential applications, *J Appl Phys*, **108**, 071301.
58. Grande L., Chundi V.T., Wei D., Bower C., Andrew P., Ryhanen T. (2012) Graphene for energy harvesting/storage devices and printed electronics, *Particuology*, **10**, 1–8.
59. Huang X., Qi X.Y., Boey F., Zhang H. (2012) Graphene-based composites, *Chem Soc Rev*, **41**, 666–686.
60. Machado B.F., Serp P. (2012) Graphene-based materials for catalysis, *Catal Sci Technol*, **2**, 54–75.
61. Kim K., Choi J.Y., Kim T., Cho S.H., Chung H.J. (2011) A role for graphene in silicon-based semiconductor devices, *Nature*, **479**, 338–344.
62. Jo G., Choe M., Lee S., Park W., Kahng Y.H., Lee T. (2012) The application of graphene as electrodes in electrical and optical devices, *Nanotechnology*, **23**, 112001.

This page intentionally left blank

Chapter 2

Electronic Band Structure and Properties of Graphene

Yihong Wu

*Department of Electrical and Computer Engineering, National University of Singapore,
4 Engineering Drive 3, Singapore 117576
elewuyh@nus.edu.sg*

2.1 Lattice structure

The peculiar electronic properties of graphene originate from its unique lattice structure. Graphene has a single layer of carbon atoms arranged in a honeycomb lattice, as shown in Fig. 2.1a. The primitive cell spanned by the following two lattice vectors

$$\vec{a}_1 = \left(\frac{3}{2}a, -\frac{\sqrt{3}}{2}a \right), \quad \vec{a}_2 = \left(\frac{3}{2}a, \frac{\sqrt{3}}{2}a \right) \quad (2.1)$$

contains two atoms, one of type A and the other of type B, which represent the two triangular lattices. Here, $a = 0.142$ nm is the carbon bond length. Type A atoms occupy the lattice sites $\vec{R} = m\vec{a}_1 + n\vec{a}_2$, where m and n are integers, and the B atoms are shifted with respect to the A atoms in each primitive cell by $\vec{\tau} = (\vec{a}_1 + \vec{a}_2)/3$.

Two-Dimensional Carbon: Fundamental Properties, Synthesis, Characterization, and Applications

Edited by Yihong Wu, Zexiang Shen, and Ting Yu

Copyright © 2014 Pan Stanford Publishing Pte. Ltd.

ISBN 978-981-4411-94-3 (Hardcover), 978-981-4411-95-0 (eBook)

www.panstanford.com

The corresponding reciprocal lattice vectors are given by

$$\bar{g}_1 = \frac{4\pi}{3\sqrt{3}a} \left(\frac{\sqrt{3}}{2}, -\frac{3}{2} \right), \quad \bar{g}_2 = \frac{4\pi}{3\sqrt{3}a} \left(\frac{\sqrt{3}}{2}, \frac{3}{2} \right) \quad (2.2)$$

which also form a honeycomb lattice, but appears to be rotated by 30° when compared with the real lattice. The first Brillouin zone (BZ) is a hexagon with a side length of $\frac{4\pi}{3\sqrt{3}a}$. Inside the first BZ, points

$$\bar{K} = \left(\frac{2\pi}{3a}, \frac{2\pi}{3\sqrt{3}a} \right) \quad \text{and} \quad \bar{K}' = \left(\frac{2\pi}{3a}, -\frac{2\pi}{3\sqrt{3}a} \right)$$

are of particular interest, where, as it will become clear later, the A and B lattices decouple, forming the so-called Dirac point.

2.2 Electronic Band Structure

2.2.1 Tight-Binding Model

In the ground state, each carbon has four valence electrons, two in the 2s sub-shell and two in the 2p sub-shell. When forming bonds with other carbon atoms, an individual carbon atom will first promote one of its 2s electrons into its empty 2p orbital and then form bonds with other carbon atoms via sp hybrid orbitals. In case of graphene, two 2p orbitals (p_x and p_y) hybridize with one 2s orbital to form three sp^2 hybrid orbitals, and during this process the other 2s electron is promoted to the $2p_z$ orbital. The hybrid orbits are given by

$$\begin{aligned} \phi_1^i &= \frac{1}{\sqrt{3}} s^i + \frac{\sqrt{2}}{\sqrt{3}} p_x^i \\ \phi_2^i &= \frac{1}{\sqrt{3}} s^i - \frac{1}{\sqrt{6}} p_x^i + \frac{1}{\sqrt{2}} p_y^i \\ \phi_3^i &= \frac{1}{\sqrt{3}} s^i - \frac{1}{\sqrt{6}} p_x^i - \frac{1}{\sqrt{2}} p_y^i \\ \phi_4^i &= p_z^i, \end{aligned} \quad (2.3)$$

where s , p_x , p_y , and p_z are the valence orbitals before hybridization and $i = A$ and B , indicating the A and B atoms in the honeycomb lattice. The three sp^2 hybrid orbitals lie in the xy plane and form

an angle of 120° with one another. In contrast, the $2p_z$ orbital is perpendicular to the xy plane. Due to the strong directionality of the sp^2 hybrid orbitals, they subsequently form the so-called σ bonds with the three nearest neighbor carbon atoms in the honeycomb lattice. The σ bonds are energetically stable and localized; therefore, they do not contribute to the electrical conduction. The overlap of the $2p_z$ orbitals of neighboring carbon atoms leads to the formation of π -bonds and anti-bonds (π^*), which are responsible for the high electrical conductivity of graphene.

The band structure of graphene can be calculated using the tight-binding approximation by taking into account only the p_z orbitals [1, 2]. The calculation involves the construction of a wave function which is the linear combination of Bloch wave functions for A and B atoms and the use of variational principle to obtain the eigenfunctions and eigenstates. Under this framework, the single-particle electron wavefunction in a crystal can be written as

$$\Psi_{\vec{k}}^{(n)} = \sum_{\alpha i} C_{\alpha i}^{(n)} \chi_{\vec{k}\alpha i}(\vec{r}), \quad (2.4)$$

where n is the band index, \vec{k} is the wave vector, α is the index of orbitals for each atom, i is the index of atoms in a primitive cell, $C_{\alpha i}^{(n)}$ is the coefficient to be determined, and $\chi_{\vec{k}\alpha i}(\vec{r})$ is a linear combination of atomic orbitals which satisfies the Bloch's theorem:

$$\chi_{\vec{k}\alpha i}(\vec{r}) = \frac{1}{\sqrt{N}} \sum_{\vec{R}_l} e^{i\vec{k}\cdot\vec{R}_l} \phi_{\alpha}(\vec{r} - \vec{t}_i - \vec{R}_l) \quad (2.5)$$

with the summation running over all primitive cells (N in this case) of the crystal. Here, \vec{r} is the position vector, \vec{t}_i is the position of atom i in a specific primitive cell, and \vec{R}_l is the position of the l th primitive cell. In case of graphene, $i = A$ and B and α can be omitted because we are only interested in the p_z orbital; therefore, $\chi_{\vec{k}\alpha i}(\vec{r})$ can be written as

$$\chi_{\vec{k}A}(\vec{r}) = \frac{1}{\sqrt{N}} \sum_{\vec{R}_l} e^{i\vec{k}\cdot\vec{R}_l} p_z(\vec{r} - \vec{t}_A - \vec{R}_l) \quad (2.6)$$

for atom A and

$$\chi_{\vec{k}B}(\vec{r}) = \frac{1}{\sqrt{N}} \sum_{\vec{R}_l} e^{i\vec{k}\cdot\vec{R}_l} p_z(\vec{r} - \vec{t}_B - \vec{R}_l) \quad (2.7)$$

for atom B. The linear combination of these two gives

$$\Psi_{\vec{k}}^{(n)} = C_A^{(n)} \chi_{\vec{k}A}(\vec{r}) + C_B^{(n)} \chi_{\vec{k}B}(\vec{r}). \quad (2.8)$$

By substituting Eq. (2.8) into Schrödinger equation and minimizing the energy, one obtains the following secular equation:

$$\begin{bmatrix} H_{11} - \varepsilon_{\vec{k}}^{(n)} & H_{12} \\ H_{21} & H_{22} - \varepsilon_{\vec{k}}^{(n)} \end{bmatrix} \begin{bmatrix} C_{\vec{k}A}^{(n)} \\ C_{\vec{k}B}^{(n)} \end{bmatrix} = 0. \quad (2.9)$$

Here, $\varepsilon_{\vec{k}}^{(n)}$ is the energy and $H_{\alpha\beta}$ ($\alpha, \beta = 1, 2$) are the interaction matrix elements. The latter can be readily obtained by taking into account the nearest neighbor interactions:

$$\begin{aligned} H_{11} &= \langle \chi_{\vec{k}A} | H | \chi_{\vec{k}A} \rangle = \sum_{\vec{R}} e^{i\vec{k}\cdot\vec{R}} \langle p_z(\vec{r} - \vec{t}_A) | H | p_z(\vec{r} - \vec{t}_A - \vec{R}) \rangle = \varepsilon_{zA} \\ H_{22} &= \langle \chi_{\vec{k}B} | H | \chi_{\vec{k}B} \rangle = \sum_{\vec{R}} e^{i\vec{k}\cdot\vec{R}} \langle p_z(\vec{r} - \vec{t}_B) | H | p_z(\vec{r} - \vec{t}_B - \vec{R}) \rangle = \varepsilon_{zB} \\ H_{12} &= \langle \chi_{\vec{k}A} | H | \chi_{\vec{k}B} \rangle = \sum_{\vec{R}} e^{i\vec{k}\cdot\vec{R}} \langle p_z(\vec{r} - \vec{t}_A) | H | p_z(\vec{r} - \vec{t}_B - \vec{R}) \rangle \\ &= -\gamma_0 - \gamma_0 e^{-i\vec{k}\cdot\vec{a}_1} - \gamma_0 e^{-i\vec{k}\cdot\vec{a}_2} \\ H_{21} &= \langle \chi_{\vec{k}B} | H | \chi_{\vec{k}A} \rangle = \sum_{\vec{R}} e^{i\vec{k}\cdot\vec{R}} \langle p_z(\vec{r} - \vec{t}_B) | H | p_z(\vec{r} - \vec{t}_A - \vec{R}) \rangle \\ &= -\gamma_0 - \gamma_0 e^{i\vec{k}\cdot\vec{a}_1} - \gamma_0 e^{i\vec{k}\cdot\vec{a}_2}. \end{aligned} \quad (2.10)$$

Here, ε_{zA} (ε_{zB}) is the energy of p_z orbital for atom A (B) after the hybridization but without the formation of bonds with neighboring atoms and γ_0 is the hopping energy between nearest neighbor atoms. As we are only interested in the excitation spectrum, we may set ε_{zA} (ε_{zB}) = 0. The electronic band structure can be obtained by letting the determinant be zero, i.e.,

$$\det \begin{bmatrix} H_{11} - \varepsilon_{\vec{k}}^{(n)} & H_{12} \\ H_{21} & H_{22} - \varepsilon_{\vec{k}}^{(n)} \end{bmatrix} = 0. \quad (2.11)$$

Solving Eq. (2.11) gives the energy dispersion:

$$E(\vec{k}) = \pm \gamma_0 \sqrt{1 + 4 \cos\left(\frac{3}{2} k_x a\right) \cos\left(\frac{\sqrt{3}}{2} k_y a\right) + 4 \cos^2\left(\frac{\sqrt{3}}{2} k_y a\right)}. \quad (2.12)$$

Note that, for clarity, we have replaced ε_k^n by $E(k)$ since we have only two bands which are corresponding to the conduction and the valence band of electrons. In Eq. (2.12), k_x and k_y are the components of \vec{k} in the (k_x, k_y) plane, $\gamma_0 = 2.75 \text{ eV}$ is the nearest-neighbor hopping energy, and plus (minus) sign refers to the upper (π^*) and lower (π) band. Figure 2.1c shows the three-dimensional electronic dispersion (left) and energy contour lines (right) in the k -space. Near the K and K' points, the energy dispersion has a circular cone shape which, to a first order approximation, is given by

$$E(\vec{k}) = \pm \hbar v_F |\vec{k}|. \quad (2.13)$$

Here $v_F = \frac{3\gamma_0 a}{2\hbar} \approx 10^6 \text{ ms}^{-1}$ is the Fermi velocity. Note that in Eq. (4) the wave vector \vec{k} is measured from the K and K' points, respectively. This kind of energy dispersion is distinct from that of non-relativistic electrons, i.e., $E(k) = \frac{\hbar^2 k^2}{2m}$, where m is the mass of electrons. The linear dispersion becomes “distorted” with increasing k away from the K and K' points due to a second order term with a threefold symmetry; this is known as the trigonal warping of the electronic spectrum in literature [3–5]. The peculiarity of electrons in graphene near the K (K') points can be intuitively understood as follows. The $2p_z$ orbital of each carbon atom in the A sub-lattice interacts with the three nearest neighboring atoms in the B sub-lattice (and vice versa) to form energy bands. Although the interaction between the two atoms is strong (as manifested by the large hopping energy), the net interaction with the three nearest neighboring atoms diminishes as \vec{k} approaches the K (K') points. This can be readily verified by substituting the $K(0, 4\pi/3\sqrt{3}a, 0)$ and $K'(2\pi/3a, 2\pi/3\sqrt{3}a, 0)$ points into Eqs. (2.10) and (2.12). The strong interaction with individual neighboring atoms makes it possible for electrons to move at a fast speed in graphene and the diminishing net interaction at Fermi level leads to a zero band gap. This result indicates that any honeycomb lattice consisting of same atoms will exhibit similar energy dispersion curves, and it is not necessary that one must have a carbon lattice.

2.2.2 Low-Energy Electronic Spectrum

Although the electronic band structure of graphene can be calculated by the tight-binding model, the salient features of low-

energy electron dynamics in graphene are better understood by modeling the electrons as relativistic Weyl fermions (within the $\vec{k} \cdot \vec{p}$ approximation), which satisfy the 2D Dirac equations [2, 6, 7].

$$\begin{aligned} -i\hbar v_F \sigma \cdot \nabla \psi &= E \psi \quad (\text{around K point}) \\ -i\hbar v_F \sigma^* \cdot \nabla \psi' &= E \psi' \quad (\text{around K' point}) \end{aligned} \quad (2.14)$$

where $\sigma = (\sigma_x, \sigma_y)$, $\sigma^* = (\sigma_x, -\sigma_y)$, $\sigma_x = \begin{bmatrix} 0 & 1 \\ 1 & 0 \end{bmatrix}$, $\sigma_y = \begin{bmatrix} 0 & -i \\ i & 0 \end{bmatrix}$, $\psi = (\psi_A, \psi_B)$, and $\psi' = (\psi'_A, \psi'_B)$. Equation (2.14) can be solved to obtain the eigenvalues and eigenfunctions (envelope functions) as follows:

$$\begin{aligned} E_\alpha &= \alpha \hbar v_F (k_x^2 + k_y^2)^{1/2} \\ \psi_{\alpha\beta}(\vec{k}) &= \frac{1}{\sqrt{2}} \begin{pmatrix} e^{-i\beta\theta_k/2} \\ \alpha e^{i\beta\theta_k/2} \end{pmatrix} \end{aligned} \quad (2.15)$$

where $\alpha = 1$ (-1) corresponds to the conduction and valence bands, $\beta = 1$ (-1) refers to the K and K' valley, and $\theta_k = \tan^{-1}(k_y / k_x)$ is determined by the direction of the wave vector in the k -space. Therefore, for both the valleys, the rotation of \vec{k} in the (k_x, k_y) plane (surrounding K or K' point) by 2π will result in a phase change of π of the wave function (so-called Berry phase) [8, 9]. The Berry phase of π has important implications to electron transport properties, which will be discussed shortly.

The eigenfunctions are two-component spinors; therefore, low-energy electrons in graphene possess a pseudospin (with $\alpha = +(-)$ 1 corresponding to the up (down) pseudospin) [10]. It is worth stressing that the pseudospin has nothing to do with the real electronic spin; the latter is an intrinsic property of electron with quantum mechanical origin, while the former is a mathematical convenience to deal with A and B atoms in graphene, which represent two intervened triangular lattices. The spinors are also the eigenfunctions of the helicity operator $\hat{h} = \frac{1}{2} \sigma \cdot \frac{\vec{p}}{|\vec{p}|}$. It is

straightforward to show that $\hat{h} \psi_{\alpha\beta} = \alpha \beta \frac{1}{2} \psi_{\alpha\beta}$. Taking \vec{n} as the unit

vector in the momentum direction, one has $\vec{n} \cdot \sigma = 1$ for electrons and $\vec{n} \cdot \sigma = -1$ for holes, for the K valley, and the opposite applies to the K' valley [11].

The unique band structure near the K point is also accompanied by a unique energy-dependence of density of states (DOS). For a 2D system with dimension $L \times L$, each electron state occupies an area of $2\pi / L^2$ in the k -space. Therefore, the low-energy DOS of graphene can

readily be found as $\frac{g_s g_v |E|}{2\pi \hbar^2 v_F^2}$, where g_s and g_v are the spin and valley

degeneracy, respectively [1, 7, 11]. The linear energy dependence of DOS holds up to $E \approx 0.3\gamma_0$, beyond which the DOS increases sharply due to trigonal warping of the band structure at higher energy [11]. Figure 2.1 compares the basic features of the electronic band structure of graphene with that of conventional 2D electron gas system [12]. In the latter case, the electron is confined in the z direction by electrostatic potentials, leading to the quantization of k_z and thus discrete energy steps. As k_x and k_y still remain as continuous, associated with each energy step is a sub-band with a parabolic energy dispersion curve. Due to energy quantization, the DOS is now given by a sum of step functions, and between the neighboring steps the DOS is constant. In contrast, graphene is a “perfect” 2D system; therefore, there are no sub-bands emerged from the confinement in the z direction. Furthermore, the single band has a linear energy dispersion in the (k_x, k_y) plane instead of a parabolic shape as it is in the case of conventional 2D system. Note that quantum wells with a well thickness of one atomic layer have been realized in several material systems; but these systems are fundamentally different from graphene. In addition to single-layer quantum wells, ultrathin 2D sheets have also been realized in many other material systems [13]. However, these nanosheets are fundamentally different from graphene either in lattice structure or in the constituent elements. Although the linear energy dispersion or Dirac points are also found to exist in some bulk materials, in most cases, they do not play a dominant role in electrical transport; therefore, it is difficult to study electron behavior in these materials directly through electrical transport measurements.

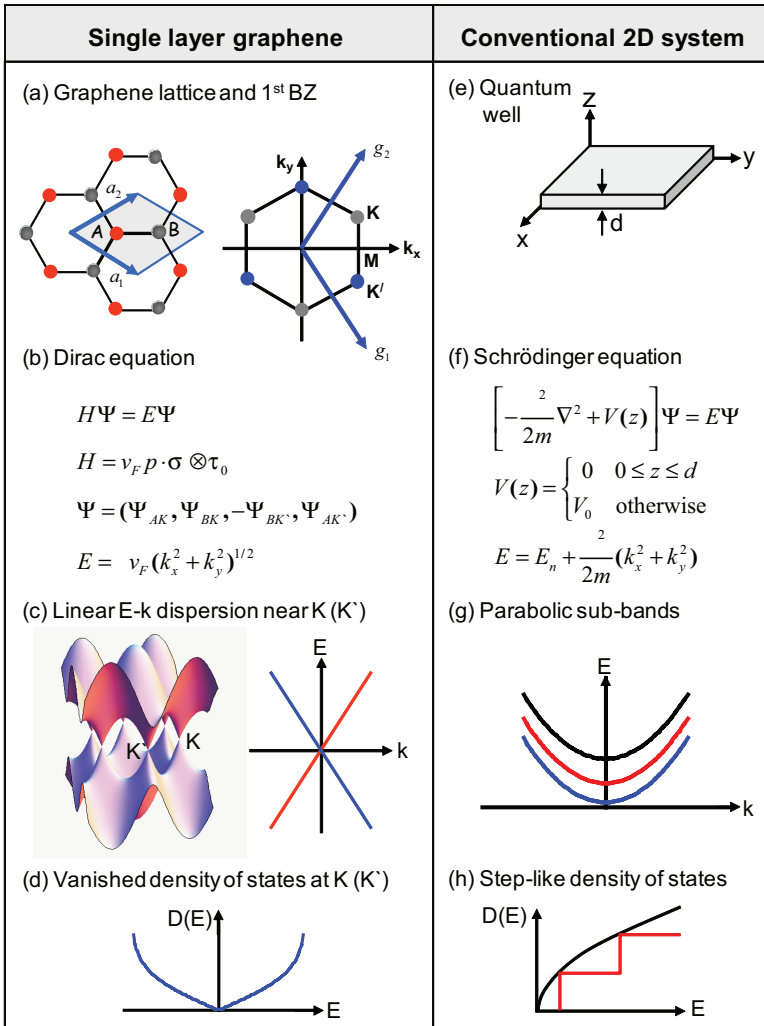


Figure 2.1 Comparison of graphene (a–d) and conventional 2D electron systems (e–h). (a) Lattice structure and first BZ; (b) Dirac equations; (c) 3D (left) and 2D (right) energy dispersions; (d) DOS as a function of energy; (e) schematic representation of a conventional 2DEG confined by electrostatic potentials in the z direction; (f) Schrödinger equation; (g) E – k dispersion curves; (h) DOS as a function of energy. Adapted and modified from Wu et al. [14].

2.2.3 Effect of Magnetic Field

The difference in the behavior of graphene and particles with a parabolic spectrum is manifested when an external magnetic field is applied perpendicularly to the plane. We first look at the case of conventional 2D electron gas system (2DEGs) [12]. Let the magnetic vector potential be $\vec{A}=(-By,0,0)$ (Landau gauge), the Schrödinger equation is given by

$$\left(\frac{\hat{p}_x - eBy}{2m_e} + \frac{\hat{p}_y^2}{2m_e} + \frac{\hat{p}_z^2}{2m_e} + V_0(z) \right) \psi = E\psi \quad (2.16)$$

where $V_0(z)$ is the confinement electrostatic potential in z direction and m_e is the electron mass. By substituting the wave function $\psi = e^{i(k_x x + k_z z)} \phi(y)$ into Eq. (2.16), one obtains

$$\left(\frac{\hat{p}_y^2}{2m_e} + \frac{1}{2} m_e \omega_c^2 (y - y_0)^2 \right) \phi = (E - E_{zn}) \phi$$

where E_{zn} is quantized energy due to confinement in z direction and $y_0 = \frac{-\hbar k_x}{eB}$. The total quantized energy levels, or Landau levels (LLs), are given by

$$E_{nl} = \left(l + \frac{1}{2} \right) \hbar \omega_c + E_{zn} \quad (2.17)$$

where $\omega_c = eB / m_e$ is the cyclotron frequency, n ($= 1, 2, 3, \dots$), and l ($= 0, 1, 2, 3, \dots$) are integers and are the indices for quantization in the z direction and LLs, respectively. The area between two neighboring LLs is $\pi(k_{l+1}^2 - k_l^2) = 2m_e \pi \omega_c / \hbar$; therefore, the degeneracy of one LL is

$$p = \frac{g_s m_e \omega_c L^2}{2\pi \hbar}, \quad (2.18)$$

where $g_s = 2$ is the spin degeneracy. In the presence of disorder, the Hall conductivity of 2DEGs exhibits plateaus at $lh/2eB$ and is quantized as $\sigma_{xy} = \pm l \frac{2e^2}{h}$ [12], leading to the integer quantum Hall effect (IQHE) [15, 16].

On the other hand, the low-energy electronic spectrum of electrons in graphene with the presence of perpendicular field is governed by

$$\begin{aligned}\hbar v_F \boldsymbol{\sigma} \cdot (-i\nabla + e\vec{A}/c)\psi &= E\psi \quad (\text{around K point}), \\ \hbar v_F \boldsymbol{\sigma}^* \cdot (-i\nabla + e\vec{A}/c)\psi &= E\psi \quad (\text{around K' point}).\end{aligned}\quad (2.19)$$

The energy of LLs has been calculated by McClure and is given by [17, 18]

$$E_l = \text{sgn}(l)v_F\sqrt{2e\hbar B|l|}. \quad (2.20)$$

Here, $|l| = 0, 1, 2, 3, \dots$ is the Landau index and B is the magnetic field applied perpendicular to the graphene plane. The LLs are doubly degenerate for the K and K' points. Compared with conventional 2DEGs, of particular interest is the presence of a zero-energy state at $l = 0$, which is shared equally by the electrons and the holes. This has led to the observation of the so-called anomalous integer quantum Hall effect, in which the Hall conductivity is given by [19, 20]

$$\sigma_{xy} = \pm 2(2l+1)\frac{e^2}{h}. \quad (2.21)$$

The measurement by Novoselov et al. [19] was performed at $B = 14$ T and temperature of 4 K. Instead of a plateau, a finite conductivity of $\pm 2e^2/h$ appeared at the zero-energy. The plateaus at higher energies occurred at half integers of $4e^2/h$. The result agrees well with Eq. (2.21). The $l = 0$ LL has also been observed in Shubnikov–de Haas oscillations at low field [19, 20], infrared spectroscopy [21, 22], and scanning tunneling spectroscopy [23–25].

2.2.4 Quantum Confinement and Tunneling

The difference in behavior between graphene and normal 2D electron system is also manifested in their response to lateral confinement by electrostatic potentials. A further confinement of 2DEGs from one of the lateral directions leads to the formation of quantum wires. For a quantum wire of size L_z and L_y in the z and y directions, the quantized energy levels are given by

$$E_{n_y, n_z} = \frac{(\hbar k_x)^2}{2m^*} + \frac{\hbar^2}{2m^*} \left(\frac{n_y \pi}{L_y} \right)^2 + \frac{\hbar^2}{2m^*} \left(\frac{n_z \pi}{L_z} \right)^2, \quad (2.22)$$

where m^* is the effective mass, k_x is the wave vector in x direction, and n_y and n_z are integers. The corresponding density of states is given by

$$\rho(E) = \frac{\sqrt{2m^*}}{\pi\hbar} \sum_{i,j} \frac{H(E - E_{n_y, n_z})}{\sqrt{E - E_{n_y, n_z}}}, \quad (2.23)$$

where H is the Heaviside function.

The counterpart of nanowire in graphene is the so-called graphene nanoribbon (GNR). In addition to the width, the electronic spectrum of GNR also depends on the nature of its edges, i.e., whether it has an armchair or a zigzag shape [26]. The energy dispersion of GNR can be calculated using the tight-binding method [26–29], Dirac equation [30, 31], or first principles calculations [32, 33]. All these models lead to the same general results, i.e., GNRs with armchair edges can be either metallic or semiconducting depending on their width, while GNRs with zigzag edges are metallic with peculiar edge or surface states. For GNRs with their edges parallel to x -axis and located at $y = 0$ and $y = L$, the energy spectra can be obtained by solving Eq. (2.19) with the boundary conditions: $\psi_B(y=0)=0$, $\psi_A(y=L)=0$ at point K and $\psi'_B(y=0)=0$, $\psi'_A(y=L)=0$ at point K' for zigzag ribbons and $\psi_A(y=0)=\psi_B(y=0)=\psi_A(y=L)=\psi_B(y=L)=0$ at point K and $\psi'_A(y=0)=\psi'_B(y=0)=\psi'_A(y=L)=\psi'_B(y=L)=0$ at point K' for armchair ribbons. The eigenvalue equations of the zigzag ribbons near the K point are given by [30]

$$e^{-2\alpha L} = \frac{k_x - \alpha}{k_x + \alpha} \quad \text{and} \quad k_x = \frac{k_n}{\tan(k_n L)} \quad (2.24)$$

where $\alpha^2 = (\hbar v_F k_x)^2 - \varepsilon^2$ for real α and $\alpha = ik_n$ for pure imaginary α , ε is the energy calculated from the Fermi level of graphene. The first equation has a real solution for α when $k_x > 1/L$, which defines a localized edge state [30]. The solution of the second equation corresponds to confined modes due to finite width of the ribbon. The eigenvalues near the K' point can be obtained by replacement, $k_x \rightarrow -k_x$ [11]. The localized edge state induces a large density of state at K and K' which are expected to play a crucial role in determining the electronic and magnetic properties of zigzag nanoribbons [26–28, 34]. In contrast, there are no localized edge states in armchair GNRs. The wave vector across the ribbon width direction is quantized by

$$k_n = \frac{n\pi}{L} - \frac{4\pi}{3\sqrt{3}a} \quad \text{and the energy is given by } \varepsilon = \pm \hbar v_F \left[k_x^2 + k_n^2 \right]^{1/2}$$

[11]. Here, n is an integer. The armchair nanoribbons will be metallic when $L = 3\sqrt{3}na/4$ and semiconducting in other cases.

Although the chiral electrons in graphene can be effectively confined in nanoribbons through the boundaries, they cannot be confined effectively by electrostatic potential barriers in the same graphene. For a one-dimensional potential barrier of height V_0 and width D in the x direction, the transmission coefficient of quasi-particles in graphene is given by [11, 35]

$$T(\phi) = \frac{\cos^2(\theta)\cos^2(\phi)}{[\cos(Dq_x)\cos\phi\cos\theta]^2 + \sin^2(Dq_x)(1 - \sin\phi\sin\theta)^2} \quad (2.25)$$

where $q_x = \sqrt{(V_0 - E)^2 / (\hbar v_F)^2 - k_y^2}$, E is the energy, k_y is the wave vector in y direction, $\phi = \tan^{-1} \frac{k_y}{k_x}$, and $\theta = \tan^{-1} \frac{k_y}{q_x}$. The

transmission coefficient becomes unity (i) when $Dq_x = n\pi$ with n as an integer, independent of the incident angle and (ii) at normal incidence, i.e., $\phi = 0$. In these two cases, the barrier becomes completely transparent, which is the manifestation of Klein tunneling [6, 35]. Stander et al. have found evidence of Klein tunneling in a steep gate-induced potential step, which is in quantitative agreement with the theoretical predictions [36]. Signature of perfect transmission of carriers normally incident on an extremely narrow potential barrier in graphene was also observed by Young and Kim [37]. Very recently, Klein tunneling was also observed in ultraclean carbon nanotubes with a small bandgap [38]. On the other hand, Dragoman has shown that both the transmission and reflection coefficients at a graphene step barrier are positive and less than unity [39]; therefore it does not support the particle–antiparticle pair creation mechanism predicted by the theory. Further concrete evidence is required to verify the Klein paradox in graphene system.

Figure 2.2 summarizes graphene and normal electron systems under an external magnetic field, in ribbon and wire form. and with a 1D potential barrier. The fundamental properties of graphene summarized in Figs. 2.1 and 2.2 lead to the peculiar electronic, magnetic, and optical properties. In the following text, we give an overview of electrical transport properties that have more experimental results to support the theoretical predictions.